Contents lists available at ScienceDirect

Chemical Engineering Research and Design

journal homepage: www.elsevier.com/locate/cherd

Insights into the transition from plug to slug flow in a horizontal pipe: An experimental study

M. Abdulkadir[a,*], D. Zhao[b], L.A. Abdulkareem[c], N.O. Asikolaye[d], V. Hernandez-Perez[e]

[a] Chemical Engineering Department, Federal University of Technology, Minna, Nigeria
[b] School of Engineering, London South Bank University, London, United Kingdom
[c] Petroleum Engineering Department, College of Engineering, University of Zakho, Iraq
[d] Petroleum Engineering Department, African University of Science and Technology, Abuja, Nigeria
[e] Department of Mechanical Engineering, Faculty of Engineering, National University of Singapore, Singapore

ARTICLE INFO

Article history:
Received 29 May 2020
Received in revised form 24 July 2020
Accepted 25 August 2020
Available online 1 September 2020

Keywords:
Gas–liquid flow
Horizontal
Void fraction
Plug-to-slug flow
ECT
Drift-flux analysis

ABSTRACT

A thorough understanding of the behaviour of the transition from plug to slug flow is imperative based on the fact that the transition can trigger an abrupt radial pressure variation. This can bring about major vibrations to the pipeline and also lead to big differences in pressure gradient and wall temperature. Unfortunately, the transition from plug to slug flow is poorly understood due to the scarce availability of experimental data. Furthermore, a considerable amount of research on the transition from plug to slug flow in the literature is based on an air–water system. In this work, the transition behaviour from plug to slug flow in a horizontal pipeline was experimentally investigated using electrical capacitance tomography (ECT). Working fluids are air–silicone oil. The work was carried out over a range of liquid and gas superficial velocities of 0.05–0.47 m/s and 0.05–4.7 m/s, respectively. Wave growth and wave characteristics mechanisms were observed to be responsible for the transition from plug to slug flow based on the obtained experimental results. Both liquid and gas superficial velocities have a major influence also on these mechanisms. The drift flux parameters for the transition from plug to slug flow was determined. A reasonably good agreement was observed from the comparison between present experimental data against hitherto published empirical models and correlations.

1. Introduction

Horizontal gas–liquid flows are often met in nuclear reactors and the hydrocarbon transportation system in the petroleum industry. Unfortunately, horizontal flows have drawn much less attention than vertical flows. Due to the influence of buoyancy force, gas phase in horizontal gas–liquid flows could be extremely unequally distributed. Consequently, the approach of extrapolating the results obtained from vertical gas–liquid flows to horizontal flows is questionable and sometimes risky. Therefore, more research work on horizontal gas–liquid flows is needed to understand the phase interaction and provide high-quality data for industrial applications.

In the horizontal configuration, two of the most prevalent flow regimes otherwise classified as intermittent flows are plug and slug flows. Their presence in pipelines triggers a rise in pressure drop, which as a result, leads to a reduction in hydrocarbon production. According to Kong et al. (2017), plug flow exists at relatively low gas superficial velocity region (less than 0.5 m/s) and liquid superficial velocities of between 0.1 and 3.0 m/s, and when the gas flow rate increases, the transition to slug flow occurs. Slug and plug flows are known to be intrinsically unstable on a small scale owing to the presence of periodic gas pockets. They become unpredictable at some larger scale with a large difference in velocity, pressure and mass flow rate in both axial and radial directions. They are featured by the irregular presence of elongated bubbles that fill up the upper section of the pipe and liquid slugs that envelops the whole cross-sectional area of the pipe. This leads to big differences in pressure gradient and wall temperature (in case heat transfer is involved). Vibrations on the pipe can also develop.

* Corresponding author.
E-mail address: mukhau@futminna.edu.ng (M. Abdulkadir).
https://doi.org/10.1016/j.cherd.2020.08.025

Nomenclature

Symbol

C_0	Distribution coefficient, dimensionless
D	Pipe diameter, m
F	Slug/plug frequency, Hz
g	Gravity constant, 9.81 m/s^2
U_m	Mixture velocity, m/s
V_T	Structure velocity, m/s
U_{SG}	Gas superficial velocity, m/s
U_{SL}	Liquid superficial velocity, m/s
U_{gd}	Drift velocity, m/s
V_G	Actual gas velocity, m/s
Tu	Slug unit period, s
x_L	Liquid quality,$x_L = \frac{U_{SL}}{U_{SL}+U_{SG}}$
ε	Average void fraction
ρ	Density, kg/m^3
μ	Viscosity, kg/ms
σ	Surface tension, N/m

Dimensionless numbers

Eotvos number $Eo = \frac{D^2 g \rho}{\sigma}$

Inverse velocity number $N_F = \frac{D^{3/2} g^{1/2} \rho}{\mu} = \left[\frac{Eo^3}{Mo}\right]^{-25}$

Morton number $Mo = \frac{g\eta^4}{\rho\sigma^3}$

Strouhal number $St = \frac{FD}{U_{SG}}$

Subscripts

G	Gas phase
L	Liquid phase
M	Mixture

Besides, the presence of these small bubbles according to Barnea et al. (1980) and Talley et al. (2015) can provide a large interfacial area for mass, momentum and energy transfer. Also, a significant number of the reported transition from plug to slug flow data in the literature have restricted use as they employ air–water as the operating fluids. Therefore, there is a need for further work to be carried out to examine the transition from plug to slug flow using system fluid other than air–water.

The irregularity of the plug/slug flow pattern can cause accidents in the oil and gas industry. The unsteady and irregular nature associated with plug and slug flow must, therefore, be taken into account in the design of two-phase gas–liquid flow systems. The knowledge on the transition from plug to slug flow is overly vital as the transition could trigger unexpected radial pressure variations and trigger serious vibrations to the pipeline. In the last two decades, the study of the transition from plug to slug flow has been the primary focus in the transportation of oil and gas. Al-Safran (2009) reported that the observed momentum occurring during the appearance of liquid and elongated bubbles produce a strong vibration and mechanical force on the pipeline. He concluded that the presence of plugs/slugs introduces structural issues that lead to cracks and accelerates the corrosion rates in the pipe. Thus, understanding the horizontal gas–liquid plug-to-slug flow is therefore, requisite to correctly model hydrocarbon transportation system.

According to Nydal et al. (1992), Hurlburt and Hanratty (2002) and Kadri et al. (2009), it is important to distinguish slug flow from plug flow as a consequence of the established differences in lengths and frequencies of gas slugs and liquid slugs as well as the differences in the population of small bubbles. Barnea et al. (1980) proposed a measure of gas bubbles-free in the liquid slugs to distinguish these two flow regimes. Based on the difference in interfacial structures in plug and slug flows, Kong and Kim (2017) claimed that the transition mechanisms from plug to slug flow might be different. A full understanding of the underlying mechanism for the transition from plug to slug flow is very limited. The flow transition is worthwhile for further investigation.

In this work, the transition mechanism from plug to slug flow was investigated in a horizontal pipe using electrical capacitance tomography (ECT). Silicone oil rather than water was chosen as working fluid as the physical properties of silicone oil are closer to those of light crude oil and can better mimic the scenarios in industry applications. The gas phase is air.

Table 1 – Properties of the air–silicone oil mixture at an operating temperature of 20 °C and at a pressure of 1 bar Abdulkadir et al. (2016).

Fluid	Density (kg/m^3)	Viscosity (kg/ms)	Surface tension (N/m)
Air	1.18	0.000018	
Silicone oil	900	0.00525	0.02

Table 2 – Experimental uncertainties associated with measurements.

Experimental measurement	Range of uncertainty
Pipe diameter (mm)	±0.5
Temperature (°C)	±0.5
Liquid superficial velocity (m/s)	±0.047
Gas superficial velocity (m/s)	±0.030
Liquid holdup	±10 % of the reading

2. Experimental facility

The experimental work was carried out in a tiltable flow rig. The representation diagram of this experimental facility is shown in Fig. 1. The pipe flow rig has been described by Azzopardi et al. (2010), and Abdulkadir et al. (2011; 2014; 2016; 2018). The test section of the pipe flow rig entails a clear acrylic pipe with an internal diameter of 0.067 m and a length of 6 m. The transparent acrylic pipe allows for direct observation of flow phenomena occurring inside the tube. The test unit can be positioned at an inclined angle to the horizontal between −5 and 90°. In this work, the rig was fixed at 0°, the horizontal position.

Silicone oil and compressed air were first mixed at the base of the rig then pumped through the riser and finally return to the air–oil separator tank Abdulkadir et al. (2016). The tank and other major components of the rig can be seen in Fig. 2. In this work, all the experiments were carried out at room temperature around 20 °C. The resulting flow patterns were determined using twin-plane electrical capacitance tomography (ECT). The twin-plane ECT sensors attached around the perimeter of the pipe were located at 4.4 and 4.489 m above the air–silicone oil mixer. This allows void fractions to be measured at two planes. The structure velocity also referred to as the translational velocity of any detected elongated bubbles and accompanying liquid plugs/slugs, can also be determined. In each run, ECT recorded void fraction data for 60 s at a frequency of 200 Hz. For a more detailed description of the pipe flow rig, the reader is referred to Abdulkadir et al. (2016).

Table 1 presents the physical properties of air and silicone oil. The determined measurement uncertainties are presented in Table 2.

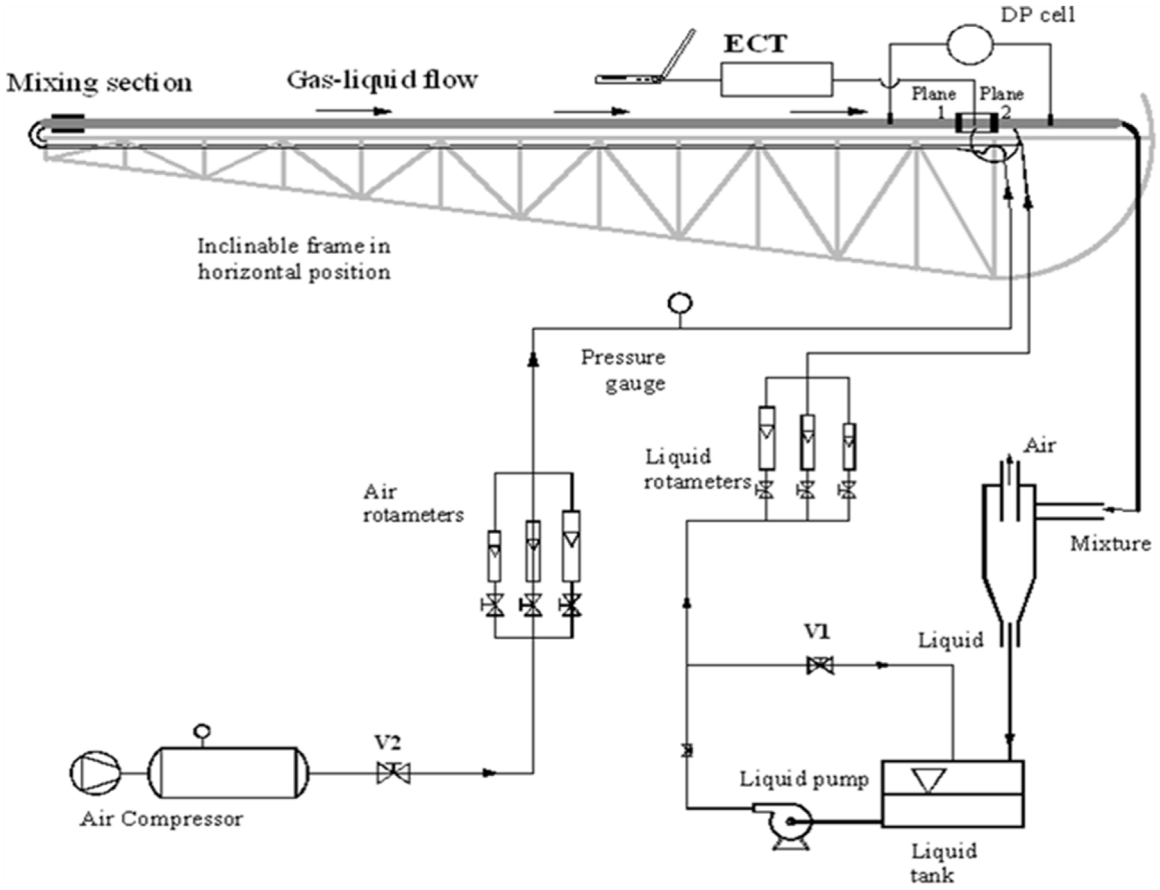

Fig. 1 – A representation illustration of the experimental rig in a horizontal position.

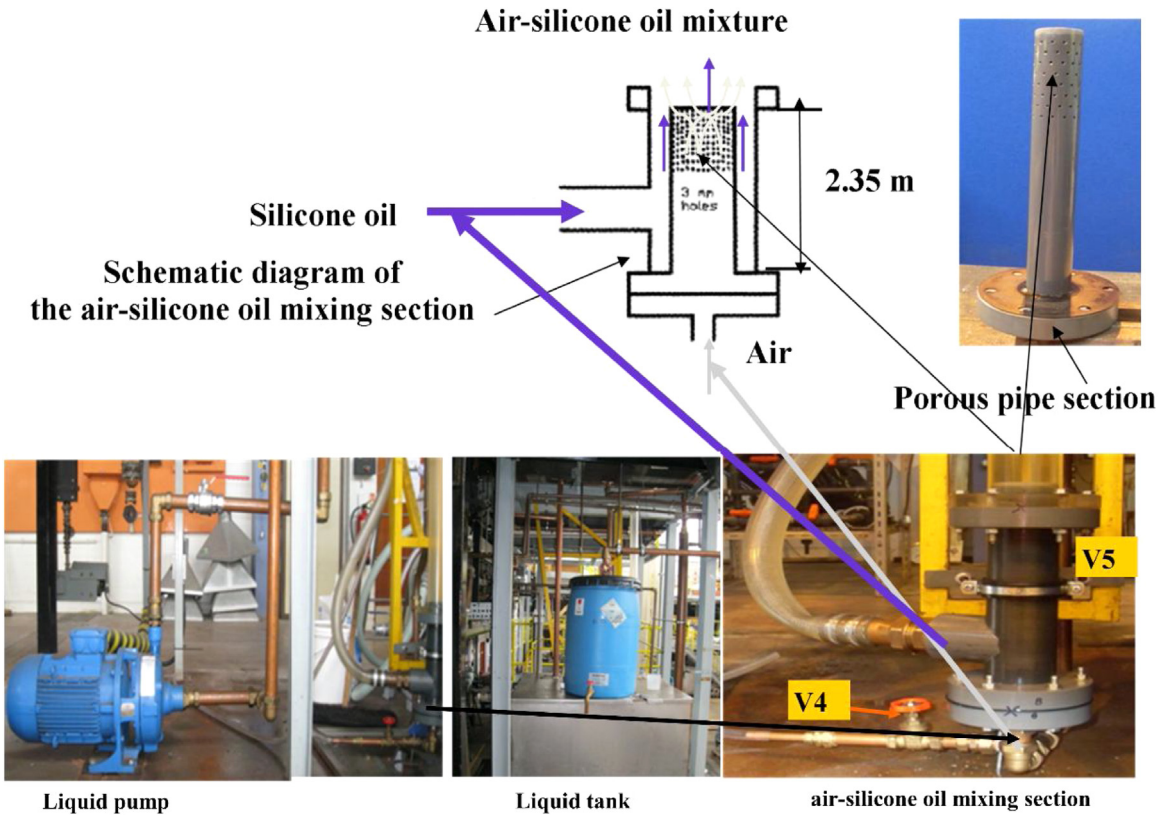

Fig. 2 – The major components of the rig.

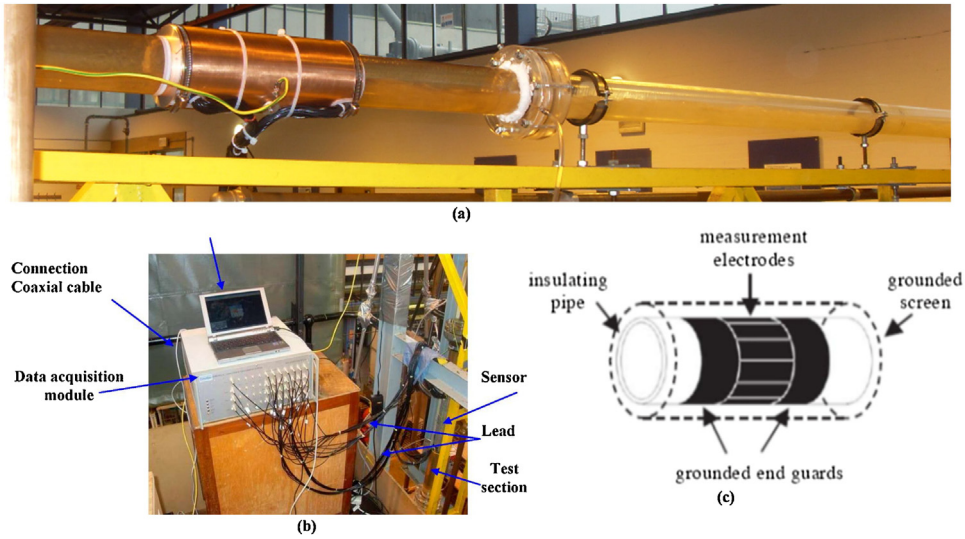

Fig. 3 – (a) The picture of the electrical capacitance tomography (ECT) sensor wound round the horizontal pipe (b) The ECT system (c) layout of driven guard electrodes Abdulkadir et al. (2014).

Table 3 – The range of variables deployed in this work.

U_{SL} (m/s)	U_{SG} (m/s)	Void fraction	Absolute error	Relative error (%)	Re_L	Re_G
0.05–0.47	0.05–4.7	0.06–0.62	0.012–0.020	1.1–3	574–5398	574–53,983

2.1. *Advanced instrumentation*

2.1.1. *Electrical capacitance tomography (ECT)*

The electrical capacitance tomography (ECT) system provided by a company called Process Tomography Limited (PTL) and shown in Fig. 3 was employed in this work to measure the void fraction. It is a PTL-300 system and consists of a data processing unit PC, DAM-200 data acquisition unit, and a capacitance sensor (Abdulkadir et al., 2020). The PC runs the ECT 32 program and the twin-plane ECT software designed for the PTL-300 system and operates supporting the Windows XP operating system. The ECT 32 program permits one or two ECT sensor planes to be controlled either independently or simultaneously, the data are captured and can be played back at different frame rates. It is worth mentioning that the measurement data can be represented as permittivity images, normalized capacitances, or a combination of both. The capacitance measurements are taken between all independent pairs of electrodes.

Multiple electrodes are arrayed around the boundary of the zone to facilitate measurements across the sensing zone. The ECT sensor, according to Wang et al. (1995) and Yang (1996), commonly consists of 8 or 12 electrodes mounted around, peripherally around the sensing zone. In this work, the ECT sensor consists of 8 electrodes. For details of the basic principles of the ECT methodology, the reader is referred to Abdulkadir et al. (2020).

3. Results and discussion

Table 3 shows the range of liquid and gas superficial velocities deployed in this work. Total 104 sets of experimental conditions were included in the measuring matrix. The corresponding flow pattern map created using the FLOPATN computer code established by Pereyra and Torres (2005) is shown in Fig. 4. The observed flow patterns in the whole experimental campaign are plug, pseudo slug flow, slug, stratified wavy, semi-annular and annular flows. However, the flow regimes under consideration in this work are plug-to-slug flows only.

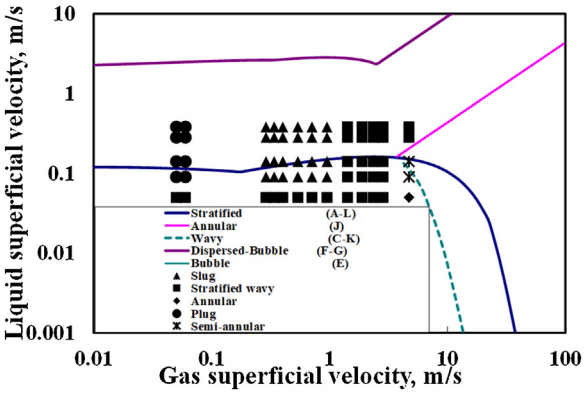

Fig. 4 – Current experimental conditions depicted in a flow pattern map as predicted by Pereyra and Torres (2005). All experimental conditions according to the figure lie in the plug, pseudo slug, slug, stratified wavy, semi-annular and annular flows region. However, the flow patterns under consideration in this work are plug–to–slug transition flow.

3.1. *The effect of fluid properties on the plug/slug flow regime using Dimensionless numbers*

In this work, three dimensionless numbers (parameters) are used to describe the rise velocity of the plug/slugs. These are the:

$$\text{Morton number,} Mo = \frac{g\mu^4}{\rho\sigma^3} \quad (1)$$

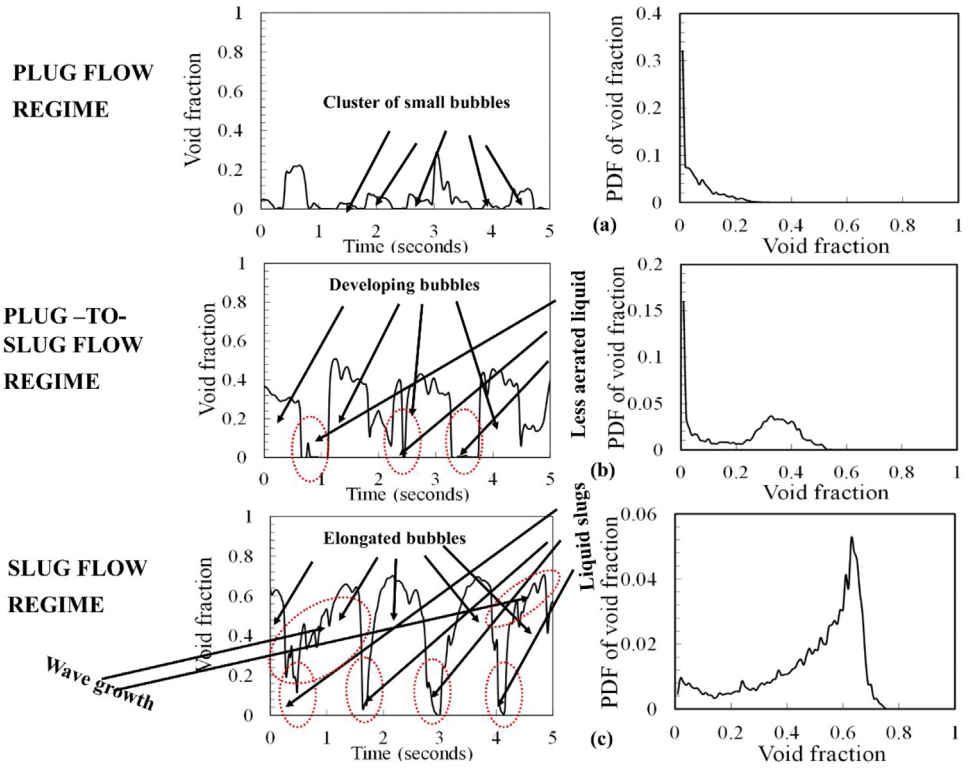

Fig. 5 – Typical PDF of void fraction, interfacial behaviour and time series of void fraction plots for (a) plug flow (b) pseudo–slug flow (c) slug flow.

Table 4 – Dimensionless numbers determined from present work at 1 bar and at the operating temperature of 20 ± 0.5 °C.

Dimensionless numbers
Eotvos number, *Eo* 1982
Morton's number, *Mo* 0.000001035
Dimensionless inverse viscosity, N_F 9312

$$\text{Eotvos number}, Eo = \frac{D^2 g \rho}{\sigma} \quad (2)$$

$$\text{Inverse viscosity number}, N_F = \frac{D^{3/2} g^{1/2} \rho}{\mu} = \left[\frac{Eo^3}{Mo}\right]^{0.25} \quad (3)$$

where, g represents the gravitational acceleration constant, D is the pipe internal diameter and σ, ρ, and μ are the surface tension of the liquid, density and viscosity, respectively.

The values of Eo, Mo, and N_F determined from the present work are presented in Table 4. From the table, the values of Eo, Mo, and N_F are 1982, 1.035×10^{-6}, and 9313, respectively. Following Eo > 100 and Mo < 10^{-6}, plugs/slugs are expected to be inertially dominated and to move at their maximum velocity. This observation is in agreement with the conclusion of White and Beardmore (1962), who claimed that the effects of the viscous and surface tension forces are negligible when Eo > 100 and Mo < 10^{-6} and that they both play little role in determining the plug/slug rise velocity.

On the matter of N_F, the value obtained in the present work is 9312, which is larger than 2. It follows, therefore, from the determined value of N_F that the effect of surface tension is negligible and that the rise velocity of the plugs/slugs is determined exclusively by liquid inertia. This observation is consistent with the findings of Fabre and Line (1992), who claimed that for surface tension forces to be relevant, $N_F < 2$.

3.2. *Flow regime recognition*

3.2.1. *Flow pattern recognition from void fraction data*

The time series of void fractions and the feature of its probability density function (PDF) have been used to categorise the flow patterns in a similar way as Costigan and Whalley (1997). 5 s of void fraction data for typical plug flow, plug to slug and slug flow are shown in Fig. 5. To the right of the void fraction plot is the corresponding probability density function (PDF) of the time series of the measured void fractions. According to Abdulkadir et al. (2014), the PDF was determined by counting the number of data points in bins of width 0.01 centred on void fractions from 0.005, 0.015. . ..0.995, and then dividing each sum by the total number of data points.

Fig. 5(a) represents the interfacial behaviour, time trace and PDF of the void fraction at the gas and liquid superficial velocities of 0.05 and 0.47 m/s, respectively. The time series shows a cluster of alternating small bubbles with a void fraction well below 0.2 but with two bubbles which normally do not have a void fraction exceeding 0.3. The small bubbles are parted by almost 100% liquid. The PDF of the void fraction, on the other hand, displays a single peak at a low void fraction of about 0.01. This flow pattern shows the characteristic signature of plug flow.

When these small bubbles in Fig. 5(a) coalesce, cap bubbles are formed as depicted in Fig. 5(b). When the gas superficial velocity increases to 0.29 m/s as shown in Fig. 5(b), the time series of void fraction shows that there exist large alternating bubbles with a rag-type shape with a void fraction alternating between 0.4 and 0.5 separated by almost 97% liquid. The

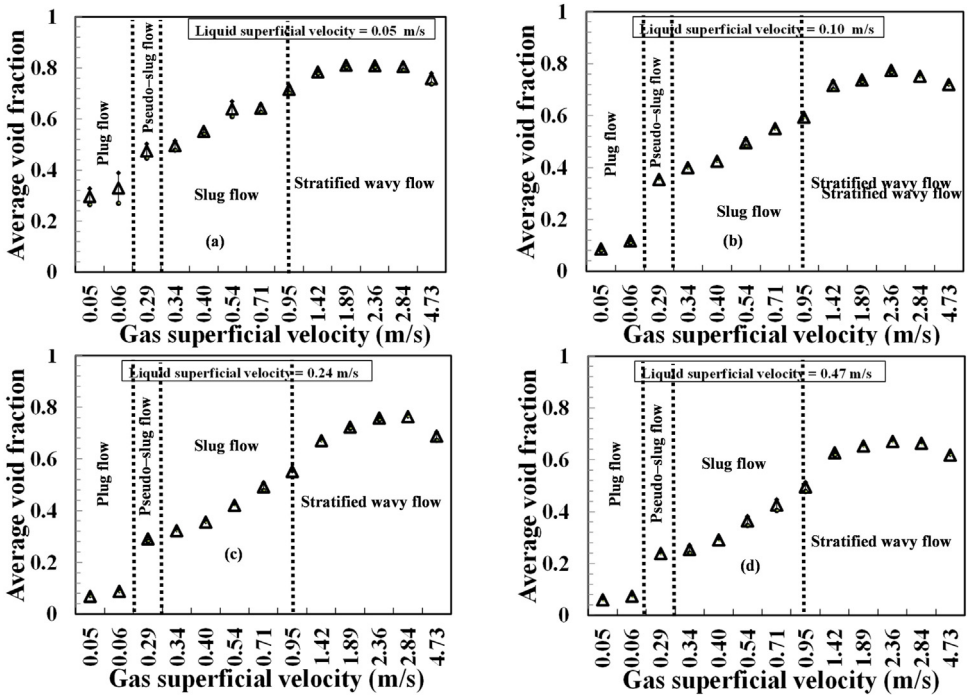

Fig. 6 – Variation of average void fraction with gas superficial velocity at liquid superficial velocities (m/s) of: (a) 0.05 (b) 0.10 m/s (c) 0.24 and (d) 0.47 m/s. The bars symbolize the standard deviation of all measurements carried out.

large bubbles are formed when the small bubbles in Fig. 5(a) coalesce owing to wave growth and wave coalescence. The mechanisms of wave growth and coalescence can be observed in Fig. 5(b). Also, it can be seen from the figure that increasing the gas superficial velocity significantly increases the number of developing bubbles in the pseudo-slug flow, which is provoked by the strong shear between the gas slug and liquid film. On the other hand, the PDF of void fraction shows two peaks, one at a void fraction of 0.001 while the other at 0.36. The figure depicts the characteristic features of both plug and slug flows, otherwise known as transitional flow (pseudo-slug flow). All these agree with the explanations described by Pawloski et al. (2004) for an air–oil two-phase flow in a horizontal pipe.

When the gas superficial velocity is gradually raised to 0.95 m/s, the cap bubbles shown in Fig. 5(b) coalesce to form elongated bubbles with a rag-type shape shown in Fig. 5(c). The elongated bubbles have a void fraction of about 0.7 and are separated by almost 90% liquid. The large elongated bubbles are formed due to wave growth and wave coalescence, which are indicated in Fig. 5(c). Also, a significant number of small bubbles as shown in Fig. 5(c), can be seen in the liquid slug, which differentiates slug flow from plug flow. It is worth mentioning that according to Barnea et al. (1980), Talley et al. (2015) and Kong and Kim (2017), the presence of these small bubbles in the air–water system can provide a large interfacial area for interfacial mass, momentum and energy transfer. The PDF of void fractions, on the other hand, depicts two peaks, a large one at a void fraction of about 0.63, and a smaller one at a low void fraction of 0.03. According to Costigan and Whalley (1997), this is the signature of slug flow.

Many works of literature like Pawloski et al. (2004) reported that a peak at low void fraction represents the tube filled with oil. This occurs when a slug passes the sensor. The higher void fraction represents the tube containing both air and oil in a stratified flow. For plug flow, the PDF of void fractions has a single peak at a low void fraction as a consequence of the tube being occupied by silicone oil.

3.3. *Void fraction*

3.3.1. *Effect of liquid and gas superficial velocities on void fraction*

Fig. 6 presents the average void fractions gathered over 60 s for liquid and gas superficial velocities of 0.05–0.47 m/s and 0.05–4.73 m/s, respecively. Four flow patterns are observed generally in the figure: $0.06 \leq \varepsilon \leq 0.33$ representing plug flow; $0.23 \leq \varepsilon \leq 0.47$ representing pseudo-slug flow; $0.25 \leq \varepsilon \leq 0.70$ representing slug flow; $0.62 \leq \varepsilon \leq 0.78$ representing stratified wavy flow. It is seen that the average void fraction plot against gas superficial velocity depicted the same tendency. It also found that the average void fraction rises with an increase in gas superficial velocity at a given liquid superficial velocity. The increase in void fraction as a result of a rise in the number of small bubbles is provoked by the strong shear between the gas slug and liquid film. Conversely, the average void fraction decreases with a rise in the liquid superficial velocity. This is in agreement with the observations of Hernandez-Alvarado et al. (2017) and Kong et al. (2018). According to Hernandez-Alvarado et al. (2017), the decline in the average void fraction is attributed to a decrease in gas residence time owing to a rise in the liquid superficial velocity. Based on flow visualization images, Kong et al. (2018) reported that the thickness of the gas layer rises as the gas superficial velocity increases. Correspondingly, the thickness of the liquid film decreases. Increasing gas superficial velocity at a constant liquid superficial velocity leads to the transition from plug to slug flow.

3.3.2. *Measured void fractions versus void fractions obtained from empirical correlations*

The average void fraction measured by ECT is compared with those obtained from the empirical models suggested, by Gregory and Scott (1969) and Mattar and Gregory (1974). Gregory and Scott (1969) carried out experimental work concerning slug flow in a horizontal pipe with carbon dioxide–water as working fluids. On the other hand, Mattar

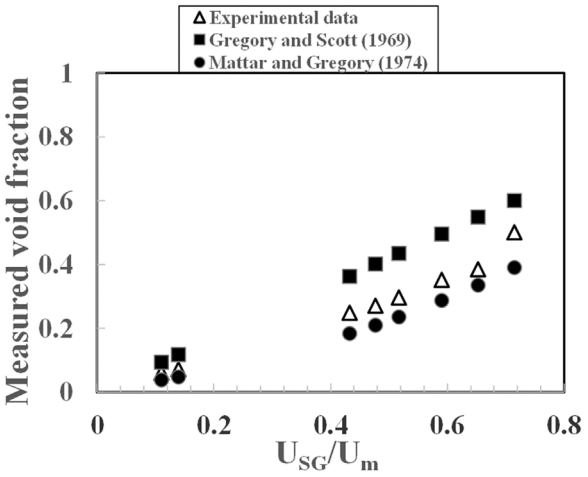

Fig. 7 – Interdependence between average void fraction and the quotient U_{SG}/U_m.

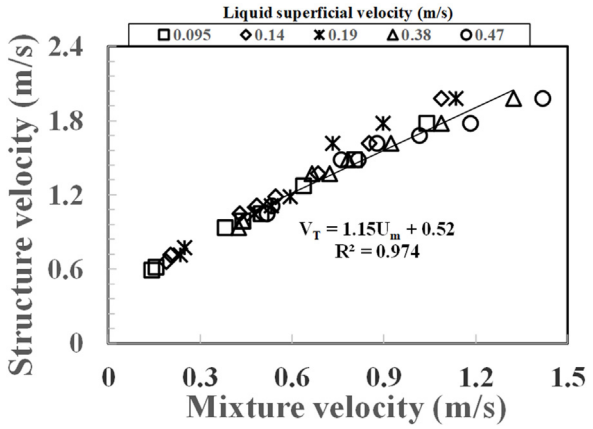

Fig. 8 – Experimentally measured structure velocity versus mixture velocity.

and Gregory (1974) developed a model especially for slug flow, at inclination angles less than 10°. The void fraction empirical models proposed by Gregory and Scott (1969) and Mattar and Gregory (1974), Eqs. (4) and (5), respectively, are as follows:

$$\varepsilon = \frac{U_{SG}}{1.19\,(U_{SL}+U_{SG})}(4) \quad (1)$$

$$\varepsilon = \frac{U_{SG}}{1.19(U_{SL}+U_{SG})+0.7}(5) \quad (2)$$

Fig. 7 depicts the interdependence between average void fraction and the quotient U_{SG}/U_m, where U_m is the mixture velocity. On the same plot, present experimental data are compared against the empirical models of Gregory and Scott (1969) and Mattar and Gregory (1974). A good agreement can be observed. The observed good agreement, therefore, suggests that the effect of pipe diameter and fluid properties is insignificant. Also, the two empirical models seem to depict a linear tendency. A similar observation was recently reported by Szalinski et al. (2010) in the situation of a vertical slug flow.

From Fig. 7, both models agree well with experimental data at a very low void fraction for $0.1 \leq \frac{U_{SG}}{U_m} \leq 0.15$. For $0.4 \leq \frac{U_{SG}}{U_m} \leq 0.73$, the experimental values agree well but lower than those predicted by the empirical model Gregory and Scott (1969). The working fluids used in Gregory and Scott (1969) are carbon dioxide and water. The different properties in the gas phase may partly contribute to the disagreement. Based on Fig. 7, the correlation from Mattar and Gregory (1974) for slug flow gave better agreement with current experimental plug-to-slug flow data. This is not surprising because the flow regime that Mattar and Gregory (1974) considered when developing their empirical model was slug flow and, similarly, the majority of the present experimental data, are in the slug flow regime. Thus, the Mattar and Gregory (1974) model is recommended for void fraction prediction in the horizontal plug to slug flow.

3.4. *Structure velocity*

The structure velocity also called the translational velocities of the elongated bubbles and accompanying liquid slugs was determined via cross-correlation methodology. The methodology involves performing a cross-correlation of the time series of the void fraction (signals) recorded from the twin-plane ECT sensors positioned 89 mm apart. For details of the cross-correlation method, the reader is referred to Abdulkadir et al. (2014; 2016). Fig. 8 shows all the calculated structure velocities for all the experimental conditions.

Fig. 8 shows a plot of the determined structure velocities of the seen elongated bubbles and liquid slugs. It can be seen from the graph that the structure velocity, U_T, appears linearly increasing with the mixture velocity, U_m. The slope obtained from the graph is the distribution coefficient, C_o, while the intercept is the drift velocity, U_{gd}. As revealed in Fig. 8, C_o and U_{gd} are 1.15 and 0.524, respectively. So, U_T, C_o and U_{gd} can be expressed as

$$U_T = 1.15U_m + 0.524 = 1.15U_m + 0.65\sqrt{gD}.(6) \quad (3)$$

The structure velocity increases with the rise of mixture velocity. A similar observation was reported by Carpintero-Rogero et al. (2006), who carried out an experimental investigation on developing plug and slug flows in a horizontal pipe employing air–water as the working fluids. It is also consistent with the findings of Nydal and Andreussi (1993), who observed that the developing slugs travel at the same velocity as regular slugs and that these velocities increase with the increase of the mixture velocity. From the plot, the effect of the liquid superficial velocity on the structure velocity is not pronounced at the low mixture velocities.

In the literature, a range of C_o values has been reported. Gregory and Scott (1969); Mattar and Gregory (1974) and Ferre (1979) reported C_o values of 1.35, 1.32 and 1.02–1.3, respectively, on the matter of horizontal and near-horizontal slug flows. Kouba (1987) claimed that for flows with low liquid and gas superficial velocities, C_o may be as high as 1.8. Zheng et al. (1994) also reported an experimental value of 1.20 for C_o for a series of slug flow conditions. Singh and Griffith (1970) reported C_o = 0.95. More recently, Abdulkadir et al. (2016) reports C_o = 1.15 for an air–silicone oil in a horizontal pipe flow. According to Nicklin et al. (1962) and Nicholson et al. (1979), however, for fully developed horizontal turbulent pipe flows a C_o value of 1.2 is usually assumed based on the fact that the ratio of the maximum to the average flow velocity in turbulent flow is approximately 1.2.

It can be observed from the graph that the intercept of the line with the y-axis is not equal to zero. This suggests that there is a drift velocity component linked with the elongated bubbles and liquid slugs. This statement corroborates the conclusions of Nicholson et al. (1979), Weber (1981), Bendiksen

Table 5 – Comparison of distribution parameter Co and Drift velocity U_{gd} obtained from present experimental data against those obtained from Zuber and Findlay (1965); Bendiksen (1984), da Silva et al. (2011) and Abdulkadir et al. (2016) correlations.

Authors	System fluid	Pipe inclination	Flow pattern	C_0	Ugd (m/s)
Zuber and Findlay (1965)	Air–water	Vertical	Slug flow	1.13	0.23
Bendiksen (1984)	Air–water	Horizontal	Slug flow	1.05	0.44
da Silva et al. (2011)	Air–water	Horizontal	Slug flow	1.18	0.34
Abdulkadir et al. (2016)	Air–silicone oil	Horizontal	Slug flow	1.24	0.45
Present experimental data	Air–silicone oil	Horizontal	Transition from plug to slug flow	1.22	0.31

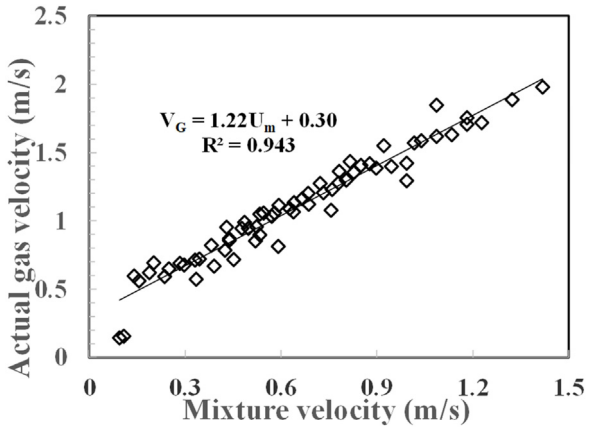

Fig. 9 – Variation of average actual gas velocity with mixture velocity.

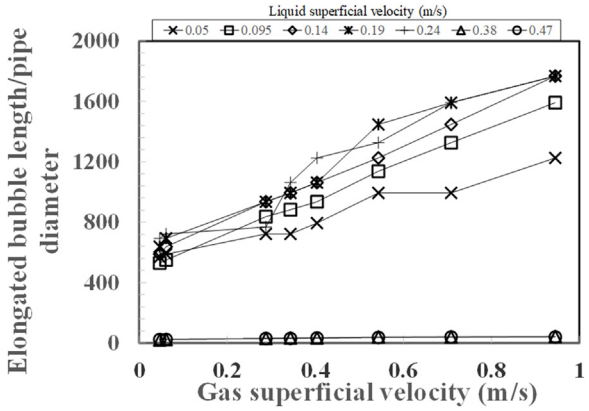

Fig. 10 – Effect of gas superficial velocity on the average elongated bubble length for various liquid superficial velocities.

(1984) and Abdulkadir et al. (2016), that a drift velocity ensues in the horizontal case.

3.5. *Drift flux analysis*

A significant number of studies have employed the drift flux approach given by Zuber and Findlay (1965) to investigate vertical flows (Ishii, 1977; Kataoka and Ishii, 1987; Hibiki and Ishii, 2002, 2003; Goda et al., 2003; Abdulkadir et al., 2018). But on the other hand, much less research has been reported on horizontal flows (Franca and Lahey, 1992; Kocamustafaogullari et al., 1994; Kong and Kim, 2017; Abdulkadir et al., 2018) due to inadequate experimental database. The drift flux analysis below provides insight on the transition from plug to slug flow in a horizontal air–silicone oil system.

According to Weber (1981), the drift-flux model is one of the most practical and accurate models for two-phase flow analysis. He concluded that the model can be used to calculate void fraction. The model relates the actual gas velocity, V_G, and the mixture velocity using two drift-flux parameters, C_0 and U_{gd}. V_G can be expressed in Eq. (7).

$$V_G = \frac{U_{SG}}{\varepsilon} = C_o U_m + U_{gd(7)} \quad (4)$$

Fig. 9 depicts a plot of actual gas velocity against mixture velocity and the best fit line. As anticipated, a linear correlation exists between them over the range of examined flow conditions. From the plot, the slope C_o and intercept U_{gd} obtained from present experimental data are 1.22 and 0.31, respectively. The correlating relationship for the experimental data is

$$V_G = C_o U_m + U_{gd} = 1.22U_m + 0.31 = 1.22U_m + 0.38\sqrt{gD}(8) \quad (5)$$

The determined C_0 value of 1.22 is close to the value of C_0 obtained from Fig. 8. It also corroborates the findings of Nydal and Andreussi (1993) that developing slugs travel at the same velocity as regular slugs and these velocities increase with increasing mixture velocity. Table 5 shows a comparison between the obtained values of C_o and U_{gd} from present experimental data against reported data of Zuber and Findlay (1965); Bendiksen (1984), da Silva et al. (2011), and Abdulkadir et al. (2016).

It can be observed from Table 5 that the $C_0$and U_{gd} valuesstated in the present work agree well with those reported in Zuber and Findlay (1965), da Silva et al. (2011), and Abdulkadir et al. (2016). Though, the present obtained C_0 value is close to those in Abdulkadir et al. (2016) and da Silva et al. (2011). On the matter of U_{gd}, according to Table 5, the present obtained value is in better agreement with those reported in Zuber and Findlay (1965) and da Silva et al. (2011). The observed differences between the present obtained values of $C_0$and U_{gd} and those reported in Zuber and Findlay (1965), da Silva et al. (2011), and Abdulkadir et al. (2016) may be partly, attributed to the fact that present work covers plug, pseudo-slug, and slug flow, while the three reported work centred on only slug flow. Different pipe diameters and working fluids may also play a part.

The non-zero intercept from Fig. 9 and Table 5 again indicates that there is a drift velocity part linked with the bubbles. The value of drift coefficient, $U_{gd}/\sqrt{gD}$, according to Bendiksen (1984), is from 0 to 0.6. The presence of drift velocity according to Benjamin (1968) is due to gravity current effects, and it is dependent on pipe internal diameter.

3.6. *Effect of liquid and gas superficial velocities on elongated bubble length*

Fig. 10 shows the influence of gas superficial velocity on the elongated bubble length at various liquid superficial velocities. The figure shows that at liquid superficial velocity of 0.05–0.24 m/s, the elongated bubble length strongly depends

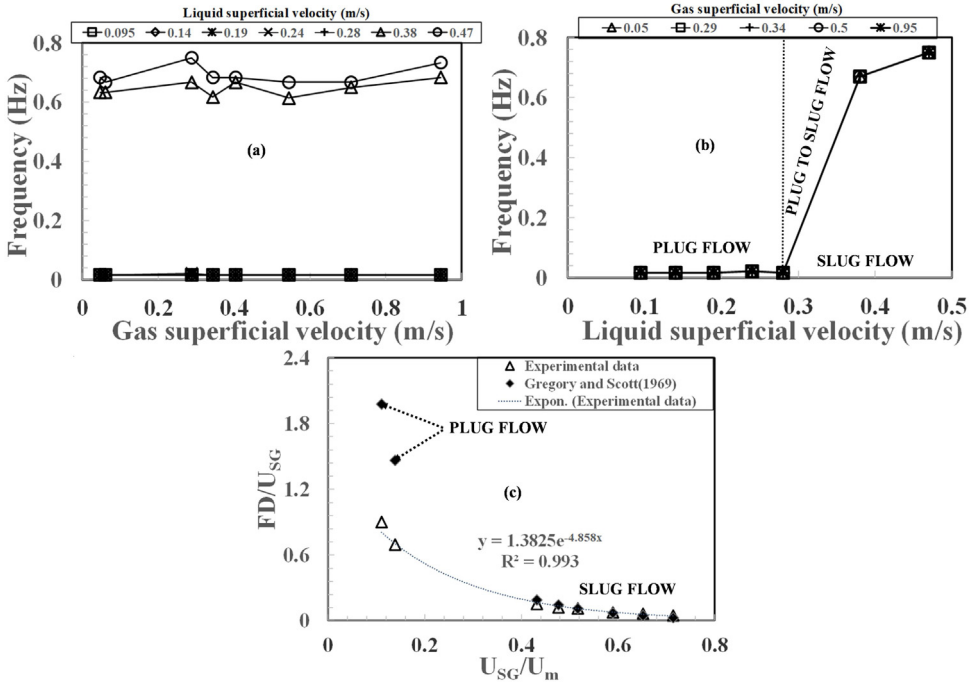

Fig. 11 – Variation of: (a) frequency with gas superficial velocity, (b) frequency with liquid superficial velocity and (c) FD/U_{SG} against U_{SG}/U_m.

on the gas superficial velocity whereby the elongated bubble length grows with an increase in gas superficial velocity.

The observed growth in the elongated bubble length may be because within these flow conditions, the bubble coalescence potential is superior to the liquid turbulent kinetic energy. This observation is in agreement with the conclusions of Kong et al. (2018), who claimed that the length of the plug/slug bubbles increases with an increase in gas superficial velocity at constant liquid superficial velocity.

This effect begins to diminish at higher liquid superficial velocities, 0.38–0.47 m/s. Within this range of liquid superficial velocities, the liquid turbulent kinetic energy is dominant over the bubble coalescence tendency. Almost all the elongated bubbles are, broken down, and as a consequence, a significant decrease in bubble length is observed. This observation is in agrees with the findings of Abdulkadir et al. (2016).

3.7. *Variation of frequency as a function of gas and liquid superficial velocities*

The slug/plug frequency F is described as the inverse of slug unit period Tu, in this work, F = 1/Tu. Fig. 11(a) shows a variation of frequency as a function of gas and liquid superficial velocity. The plot shows that the frequency weakly depends on the gas superficial velocity at the liquid superficial velocity range of 0.095–0.28 m/s. Interestingly, the dependency of frequency on gas superficial velocity becomes evident at the higher liquid superficial velocities of 0.38 to 0.47 m/s, whereby a rise in liquid superficial velocity leads to a corresponding increase in frequency. Abdulkadir et al. (2016) also reported a similar observation. Some authors, including Gregory and Scott (1969); Dukler and Hubbard (1984) and Woods and Hanratty (1999), reported a minimum in the frequency plot at the gas superficial velocity of 4 m/s but, this minimum was not seen in the present work. Fig. 11(b) shows three distinct regions based on liquid superficial velocity: 0.095–0.28 m/s, plug flow; 0.28 m/s, plug to slug transition flow; 0.39 and 0.47 m/s, slug flow.

The variation of normalized parameter FD/U_{SG} against U_{SG}/U_m at liquid superficial velocity of 0.47 m/s is depicted in Fig. 11(c), where F is the frequency and D is the pipe diameter. Seen in Fig. 11c is an exponential trend characteristic of slug flow, and the present data at values of U_{SG}/U_m between 0.1 and 0.74 agree well with the values obtained using the correlation in Gregory and Scott (1969). The observed agreement between the two values may be because both the present work and that of Gregory and Scott (1969) covers slug flow. It is worth mentioning, however, that at low U_{SG}/U_m, there are two significant variations in the values of FD/U_{SG} obtained. The variations can be described by the reality that within those values, the ensuing flow pattern is plug flow while the correlation was developed for slug flow.

Three dimensionless parameters Strouhal number St, liquid volume x_L and Lockhart-Martinelli parameter X were used to process the average slug/plug frequency and consequently plotted in Fig. 12, in which St is presented as a function of x_L (Fig. 12a) and St also presented as a function of X (Fig. 12b). It can be seen from the figure that both St and x_L can be associated with the Fossa et al. (2003) Eq. (12):

$$St = \frac{FD}{U_{SG}} \quad (9) \tag{6}$$

$$x_L = \frac{U_{SL}}{U_{SL} + U_{SG}} \quad (10) \tag{7}$$

$$X = \sqrt{\frac{\rho_L}{\rho_G}\frac{U_{SL}}{U_{SG}}} \quad (11) \tag{8}$$

$$St = \frac{0.05x_L}{1 - 1.675x_L + 0.768x_L^2} \quad (12) \tag{9}$$

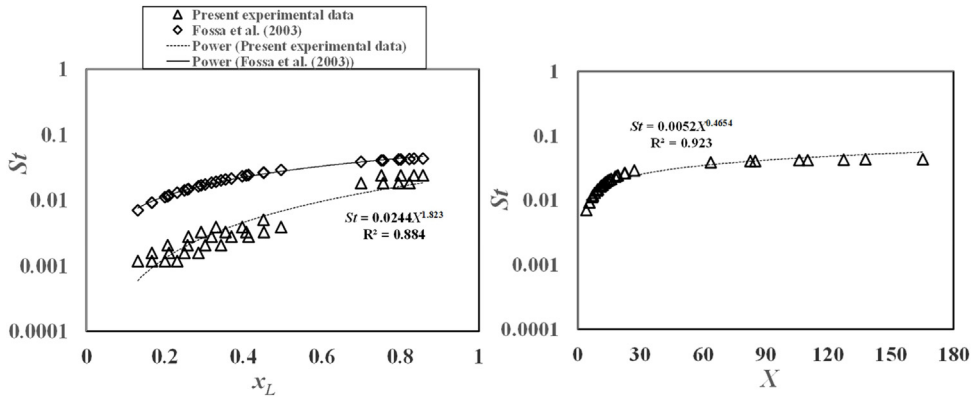

Fig. 12 – A logarithmic plot of the Strouhal number *St* versus (a) the liquid volume fraction x_L and (b) the Lockhart–Martinelli parameter *X*.

4. Conclusion

Electrical capacitance tomography (ECT) was successfully deployed to investigate the hydrodynamic behaviour in the transition from plug to slug flow in a horizontal 6 m long and 67 mm internal diameter pipe. The acquisition frequency of the ECT is 200 Hz. Working fluids are air and silicone oil. The experimental campaign was carried out for a series of liquid and gas superficial velocities of 0.05–0.47 m/s and 0.05–4.7 m/s, respectively. The signals from the twin-plane ECT were processed to get the time series of void fraction, frequency, and structure velocity. The summary of the key findings from this work are as follows:

1 The four identified flow patterns from the plot of average void fraction against gas superficial velocity are: $0.06 \leq \varepsilon \leq 0.33$ plug flow; $0.23 \leq \varepsilon \leq 0.47$ pseudo-slug flow; $0.25 \leq \varepsilon \leq 0.70$ slug flow; $0.62 \leq \varepsilon \leq 0.78$ stratified wavy flow.
2 The increase in void fraction was because of the strong shear between the liquid slug and liquid film. Conversely, the decrease in void fraction was triggered by a rise in the liquid superficial velocity.
3 The comparison between present data against reported models and correlations exhibited reasonably good agreement.
4 The slope C_o and intercept U_{gd} obtained using the drift flux analysis are 1.22 and 0.31, respectively, and are seen to be close to the values obtained from the plot of structure velocity against mixture velocity.
5 At higher liquid superficial velocities of 0.38–0.47 m/s, bubble breakup mechanism became dominant and as a result most of the elongated bubbles collapsed.
6 The plot of plug/slug frequency showed three distinct regions based on liquid superficial velocity: 0.095–0.28 m/s, plug flow; 0.28 m/s, pseudo-slug flow; 0.39 and 0.47 m/s, slug flow.

Conflict of interest

The authors declare that there is no conflict of interest.

Acknowledgment

Abdulkadir, M., would like to express his sincere appreciation to the Nigerian government through the Petroleum Technology Development Fund (PTDF) for providing the funding for his doctoral studies.

This work has been undertaken within the Joint Project on Transient Multiphase Flows and Flow Assurance. The Author(s) wish to acknowledge the contributions made to this project by the UK Engineering and Physical Sciences Research Council (EPSRC) and the following: - GL Industrial Services; BP Exploration; CD-adapco; Chevron; ConocoPhillips; ENI; ExxonMobil; FEESA; IFP; Institutt for Energiteknikk; PDVSA (INTEVEP); Petrobras; PETRONAS; SPT; Shell; SINTEF; Statoil and TOTAL. The Author(s) wish to express their sincere gratitude for this support.

References

Abdulkadir, M., Zhao, D., Sharaf, S., Abdulkareem, L.A., Lowndes, I.S., Azzopardi, B.J., 2011. Interrogating the effect of 90° bends on air–silicone oil flows using advanced instrumentation. Chem. Eng. Sci. 66, 2453–2467.

Abdulkadir, M., Hernandez-Perez, V., Lowndes, I.S., Azzopardi, B.J., Dzomeku, S., 2014. Experimental study of the hydrodynamic behaviour of slug flow in a vertical riser. Chem. Eng. Sci. 106, 60–75.

Abdulkadir, M., Hernandez–Perez, V., Lowndes, I.S., Azzopardi, B.J., Sam-Mbomah, E., 2016. Experimental study of the hydrodynamic behaviour of slug flow in a horizontal pipe. Chem. Eng. Sci. 156, 147–161.

Abdulkadir, M., Hernandez-Perez, V., Kwatia, C.A., Azzopardi, B.J., 2018. Interrogating flow development and phase distribution in vertical and horizontal pipes using advanced instrumentation. Chem. Eng. Sci. 186, 152–167.

Abdulkadir, M., Jatto, D.G., Abdulkareem, L.A., Zhao, D., 2020. Pressure drop, void fraction and flow pattern of vertical air–silicone oil flows using differential pressure transducer and advanced instrumentation. Chem. Eng. Res. Des. 159, 262–277.

Al-Safran, E., 2009. Investigation and prediction of slug frequency in gas–liquid horizontal pipe flow. J. Pet. Sci. Eng. 69, 143–155.

Azzopardi, B.J., Abdulkareem, L.A., Zhao, D., Thiele, S., da Silva, M.J., Beyer, M., Hunt, A., 2010. Comparison between electrical capacitance tomography and wire mesh sensor output for air/silicone oil flow in a vertical pipe. Ind. Eng. Chem. Res., 49.

Barnea, D., Shoham, O., Taitel, Y., Dukler, A.E., 1980. Flow patterns transition for gas–liquid flow in horizontal and inclined pipes. Transition of plug to slug flow and associated fluid dynamics. Int. J. Multiph. Flow 6, 217–225.

Bendiksen, K.H., 1984. An experimental investigation of the motion of long bubbles in inclined tubes. Int. J. Multiph. Flow 10, 467–483.

Benjamin, T.B., 1968. Gravity currents and related phenomena. J. Fluid Mech. 31, 209–248.

Carpintero-Rogero, E., Kroess, B., Sattel-Mayer, T., 2006. Simultaneous HS-PIV and shadowgraph measurements of gas–liquid flows in a horizontal pipe. In: 13th International

Symposium on Applications of Laser Techniques to Fluid Mechanics, Lisbon, Portugal, 26–29 June, 2006.
Costigan, G., Whalley, P.B., 1997. Slug flow regime identification from dynamic void fraction measurements in vertical air–water flows. Int. J. Multiph. Flow 23, 263–282.
da Silva, M.J., Hampel, U., Arruda, L.V.R., do Amaral, C.E.F., Morales, R.E.M., 2011. Experimental investigation of horizontal gas–liquid slug flow by means of wire mesh sensor. J. Braz. Soc. Mech. Sci. Eng. XXXIII, 237–242.
Dukler, A.E., Hubbard, M.G., 1984. A model for gas–liquid slug flow in horizontal and near horizontal tubes. Ind. Eng. Chem. Fundam. 14, 337–347.
Fabre, J., Line, A., 1992. Modelling of two-phase slug flow. Annu. Rev. Fluid Mech. 24, 21–46.
Ferre, D., 1979. Ecoulments diphasiques a poches en conduite horizontale. Rev. Ins. Fr. Pet. 34, 113–142.
Fossa, M., Guglielmini, G., Marchitto, A., 2003. Intermittent flow parameters from void fraction analysis. Flow Meas. Instrum. 14, 161–168.
Franca, F., Lahey, R.T., 1992. The use of drift-flux techniques for the analysis of horizontal two-phase flows. Int. J. Multiph. Flow 18, 787–801.
Goda, H., Hibiki, T., Kim, S., Ishii, M., Uhle, J., 2003. Drift-flux model for downward two-phase flow. Int. J. Heat Mass Transf. 46, 4835–4844.
Gregory, G.A., Scott, D.S., 1969. Correlation of liquid slug velocity and frequency in horizontal concurrent as liquid flow. AIChE J. 15, 833–835.
Hernandez-Alvarado, F., Kalaga, D.V., Turney, D., Banerjee, S., Joshi, J.B., Kawaji, M., 2017. Void fraction, bubble size and interfacial area measurements in co-current downflow bubble column reactor with microbubble dispersion. Kataoka, I. and Ishii, M., 1987. Drift flux model for large diameter pipe and new correlations for pool void fraction. Chem. Eng. Sci. 168, 403–413.
Hibiki, T., Ishii, M., 2002. Distribution parameter and drift velocity of drift-flux model in bubbly flow. Int. J. Heat Mass Transf. 45, 707–721.
Hibiki, T., Ishii, M., 2003. One-dimensional drift-flux model for two-phase flow in a large diameter pipe. Int. J. Heat Mass Transf. 46, 1773–1790.
Hurlburt, E.T., Hanratty, T.J., 2002. Prediction of the transition from stratified to slug and plug flow for long pipes. Int. J. Multiph. Flow 28, 707–729.
Ishii, M., Argonne National Laboratory, III (USA) 1977. One-dimensional drift-flux model and constitutive equations for relative motion between phases in various two-phase flow regimes.
Kadri, U., Mudde, R.F., Oliemans, R.V.A., Bonizzi, M., Andreussi, P., 2009. Prediction of the transition from stratified to slug flow or roll-waves in gas–liquid horizontal pipes. Int. J. Multiph. Flow 35, 1001–1010.
Kataoka, I., Ishii, M., 1987. Drift flux model for large diameter pipe and new correlations for pool void fraction. Int. J. Heat Mass Transf. 30, 1927–1939.
Kocamustafaogullari, G., Huang, W.D., Razi, J., 1994. Measurement and modelling of average void fraction, bubble size and interfacial area. Nucl. Eng. Des. 148, 437–453.
Kong, R., Kim, S., 2017. Characterization of horizontal air–water two-phase flow. Nucl. Eng. Des. 312, 266–276.
Kong, R., Kim, S., Bajorek, S., Tien, K., Haxie, C., 2017. Experimental study of horizontal air–water bubbly-to-plug and bubbly-to-slug transition flows in a 3.81 cm ID pipe. Int. J. Multiph. Flow 94, 137–155.
Kong, R., Adam, R., Seungjin, K., Stephen, B., Kirk, T., Chris, H., 2018. Experimental study of horizontal air–water plug-to-slug transition flow in different pipe sizes. Int. J. Heat Mass Transf. 123, 1005–1020.
Kouba, G.E., 1987. Horizontal Slug Flow Modelling and Metering. PhD Thesis. University of Tulsa.
Mattar, J., Gregory, G.A., 1974. Air oil slug flow in an upward inclined pipe-1: slug velocity, holdup and pressure gradient. J. Can. Pet. Technol. 13, 69–76.
Nicholson, K., Aziz, K., Gregory, G.A., 1979. Intermittent two phase flow in horizontal pipes, predictive models. Can. J. Chem. Eng. 56, 653–663.
Nicklin, D.J., Wilkes, J.O., Davidson, J.F., 1962. Two-phase flow in vertical tubes. Process Saf. Environ. Prot. 40, 61–68.
Nydal, O.J., Andreussi, P., 1993. Gas entrainment in liquid slugs. In: Proceedings of the 3rd International Offshore and Polar Engineering Conference, Singapore, 6–11 June, 1993.
Nydal, O.J., Pintus, S., Andreussi, P., 1992. Statistical characterization of slug flow in horizontal pipes. Int. J. Multiph. Flow 18, 439–453.
Pawloski, J.L., Ching, C.Y., Shoukri, M., 2004. Measurement of void fraction and pressure drop of air–oil two-phase flow in horizontal pipes. J. Eng. Gas Turbine Power 126, 107–118.
Pereyra, E., Torres, C., 2005. FLOPATN—Flow Pattern Prediction and Plotting Computer Code. The University of Tulsa, Tulsa, Oklahoma, USA.
Singh, G., Griffith, P., 1970. Determination of the pressure drop optimum pipe size for a two-phase slug flow in an inclined pipe. J. Eng. Ind. 92, 717–725.
Szalinski, L., Abdulkareem, L.A., da Silva, M.J., Thiele, S., Beyer, M., Lucas, D., Hernandez Perez, V., Azzopardi, B.J., Hampel, U., 2010. Comparative study of gas–oil and gas–water two-phase flow in a vertical pipe. Chem. Eng. Sci. 65, 3836–3848.
Talley, J.D., Worosz, T., Kim, S., Buchanan, J.R., 2015. Characterization of horizontal air–water two-phase flow in a round pipe part 1: flow visualization. Int. J. Multiph. Flow 76, 212–222.
Wang, S.J., Dyakowski, T., Xie, C.G., Williams, R.A., Beck, M.S., 1995. Real time capacitance imaging of bubble formation at the distributor of a fluidized bed. Chem. Eng. J. 56, 95–100.
Weber, M.E., 1981. Drift in intermittent two-phase flow in horizontal pipes. Can. J. Chem. Eng. 59, 398–399.
White, E.T., Beardmore, R.H., 1962. The velocity of rise of single cylindrical air bubbles through liquids contained in vertical tubes. Chem. Eng. Sci. 17, 351–361.
Woods, B.D., Hanratty, T.J., 1999. Influence of Froude number on physical processes determining frequency of slugging in horizontal gas–liquid flows. Int. J. Multiph. Flow 25, 1195–1223.
Yang, W.Q., 1996. Calibration of capacitance tomography system: a new method for setting measurement range. Meas. Sci. Technol. 7, 863–867.
Zheng, G.H., Brill, J.P., Shoham, O., 1994. Slug flow behaviour in a hilly terrain pipelines. Int. J. Multiph. Flow 20, 63–79.
Zuber, N., Findlay, J.A., 1965. Average volumetric concentration in two-phase flow systems. J. Heat Transf. Trans. ASME 87, 453–468.